Low Temperature Physics/Fizika Nizkikh Temperatur, 2012, v. 38, No. 3, pp. 273–277

Phase transitions in $TbMnO_3$ manganites

V. Dyakonov[1,2], A. Szytuła[3], R. Szymczak[1], E. Zubov[1,2], A. Szewczyk[1], Z. Kravchenko[2], W. Bażela[4], K. Dyakonov[1,5], A. Zarzycki[6], V. Varyukhin[2], and H. Szymczak[1]

[1] *Institute of Physics, PAS, Al. Lotników 32/46, 02-668 Warsaw, Poland*
E-mail: dyakon@ifpan.edu.pl

[2] *A.A. Galkin Donetsk Physico-Technical Institute, National Academy of Sciences of Ukraine*
72 R. Luxembourg Str., Donetsk 83114, Ukraine
E-mail: zubov@fti.dn.ua

[3] *M. Smoluchowski Institute of Physics, Jagiellonian University, Reymonta 4, 30-059, Kraków, Poland*

[4] *Institute of Physics, Technical University, Podchorążych 1, 30-084 Kraków, Poland*

[5] *A.F. Ioffe Physico-Technical Institute, 192021 St.-Petersburg, Russia*

[6] *H. Niewodniczanski Institute of Nuclear Physics PAS, 31-342 Krakow, Poland*

Received September 26, 2011

X-ray diffraction and magnetic measurements of polycrystalline and nanosize $TbMnO_3$ manganites have been performed. All the compounds studied crystallize in the orthorhombic crystal structure (space group *Pnma*) at room temperature. The nanosize manganites were synthesized with a sol-gel method at different (800 and 900°C) temperatures. The average size of synthesized nanoparticles (from 45 to 70 nm) was estimated by using the x-ray diffraction and low-temperature adsorption of argon methods. An information on the evolution of properties of $TbMnO_3$ with changing grain size, temperature and magnetic field was obtained. The crystal structure parameters of nanospecimens change slightly with changing the nanoparticle size. The peculiarities of magnetic ordering in polycrystalline and nanosize $TbMnO_3$ were compared. Magnetization and the Nèel temperature corresponding to antiferromagnetic ordering of the Tb^{3+} sublattice decrease as the particle size is reduced. The inverse magnetic susceptibility of the nanoparticle samples deviates from the Curie–Weiss law below 50 K, that is connected with the magnetic ordering of the Mn^{3+} moments. Specific heat of the nanosize samples exhibits anomalies related to the magnetic ordering of the Tb^{3+} and Mn^{3+} sublattices.

PACS: *61.05.cp* X-ray diffraction;
61.46.–w Structure of nanoscale materials;
75.75.–c Magnetic properties of nanostructures;
75.47.Lx Magnetic oxides;
73.63.Bd Nanocrystalline materials.

Keywords: $TbMnO_3$, nanoparticle sample, x-ray diffraction, magnetic ordering.

1. Introduction

Out of all the known multiferroic materials, the $REMnO_3$ manganites (RE are the rare-earth ions) have attracted considerable scientific and technological attention in the last years due to strong coupling between ferroelectricity and magnetism [1,2]. The magnetoelectric effects observed in $REMnO_3$ can be used in novel magnetoelectric devices in which the magnetic properties are electrically controlled and vice versa.

To elucidate the relationship between ferroelectricity and magnetism, the electric and magnetic properties of the $ReMnO_3$ single crystals with perovskite structure as a function of temperature and magnetic field have been studied [2–9]. In particular, the $TbMnO_3$ single crystal is found to exhibit several anomalies of both specific heat and magnetization as a function of temperature connected with the antiferromagnetic ordering of the Tb^{3+} and Mn^{3+} moments [2,7,8]. Below 28 K, the magnetic structure in the Mn^{3+} sublattice transforms from a sinusoidal incommensurate to

a spiral antiferromagnetic one related to the onset of the ferroelectric phase [9]. Neutron scattering measurements [10,11] have shown the presence of an intrinsic ferromagnetic ordering in antiferromagnetic $TbMnO_3$ at low temperatures.

The nanoparticle samples exhibit properties which are different from those of the bulk material due to increasing surface-to-volume ratio of the grains as the particle size is reduced to the nanoscale [12–15].

A main motivation for performed studies was to obtain the data concerning the magnetic properties and magnetic ordering in $TbMnO_3$ as a function of nanoparticle size, taking into account that there are no reports on such measurements.

In this paper, the preparation and characterization, the x-ray diffraction, magnetic and specific heat measurements of polycrystalline and nanoparticle $TbMnO_3$ manganites have been performed that has allowed to observe the evolution of magnetic properties with changing grain size.

2. Preparation and structural characterization of $TbMO_3$ manganites

The polycrystalline $TbMnO_3$ (denoted hereafter as the S_1 sample) was synthesized using the standard solid state reaction technique. In brief, the stoichiometric amounts of Tb_7O_{11} and MnO_2 powders with high purity were mixed and were heat-treated during three stages at temperatures of 1000, 1100, and 1150 °C for 15 h with intermediate grinding of as-obtained products. Compacted under pressure pellets were sintered in air at 1200 °C for 20 h followed by temperature decrease to the room temperature at the rate of 70 °C/h.

To date, among various synthesis techniques, the sol-gel route for synthesizing manganites provides the most inexpensive experimental tool. Key features of this process are overall simplicity and easiness of grain sizes variation. In spite of these advantages, only limited compounds such as $La_{1-x}(Ca,Sr)_xMnO_3$ have been synthesized via the sol-gel process presented, for example, in Refs. 13, 15.

Here we report, for the first time, a sol-gel process for synthesis of $TbMnO_3$ manganite with varying the grain sizes. The mixture of stoichiometric amounts of high purity Mn_3O_4 and Tb_2O_3 oxides was dissolved in acetic acid with added hydrogen peroxide. The solution of urea was added to obtained solution. This mixture was evaporated to dryness. The dry remainder was decomposed at 250–450 °C. Then the powder was thoroughly grinded, pressed into pellets and annealed at different temperatures for 20 h in air, followed by a slow cooling down to the room temperature. The nanopowders obtained after annealing at 900 and 800 °C had the average particle sizes of about 70 and 45 nm (as estimated from x-ray diffraction measurements) and are denoted hereafter as S_2 and S_3 samples, respectively.

The crystallographic structure and lattice parameters of the samples studied were determined with the room temperature x-ray powder diffraction (XRD) using a Philips PW-3710 X'PERT diffractometer with CuK_α radiation. The data were analyzed with the Rietveld-type refinement softwere FullProf program [16]. The x-ray diffraction data indicate that the samples obtained are homogeneous, single phase and have an orthorhombic crystal structure described by the space group *Pnma*. All the fitted structural parameters: lattice constants, volume and positional parameters x_i, y_i and z_i for the polycrystalline and nanosize $TbMnO_3$ manganites are listed in Table 1. A small changes in the structural parameters were found for the nanosize samples. The lattice *b* parameter increases in contrast to the *a* and *c* parameters and volume which decrease as the grain sizes are reduced.

Table 1. Structural parameters of the $TbMnO_3$ samples studied derived from room temperature x-ray diffraction data

Parameter	Sample		
	S_1	S_2	S_3
a, Å	5.8456(1)	5.8191(1)	5.8109(1)
b, Å	7.4040(2)	7.4092(3)	7.4116(3)
c, Å	5.2995(1)	5.2860(2)	5.2830(1)
V, Å^3	229.37(1)	227.90(5)	227.52(2)
Tb: *x*	0.0806(2)	0.0808(2)	0.0806(1)
z	–0.1727(3)	–0.0167(3)	–0.0154(2)
O1: *x*	0.469(2)	0.472(2)	0.465(1)
z	0.101(2)	0.101(2)	0.107(2)
O2: *x*	0.329(2)	0.315(2)	0.311(1)
y	0.0525(11)	0.051(1)	0.0549(8)
z	0.705(2)	0.704(2)	0.695(1)
R_{Bragg}, %	6.64	8.51	9.23
R_{prof}, %	7.35	8.93	11.1

To estimate the grain sizes of the nanopowders obtained two methods were used: low-temperature adsorption of argon and x-ray diffraction measurements. The method of low-temperature adsorption of argon, known as BET's method [17], has allowed to determine the specific surface (S_{SS}). The average particles sizes $\langle d \rangle$ were calculated using the expression $S_{SS} = 1/(\langle d \rangle \sigma_\gamma)$ and knowing the x-ray density $\sigma_\gamma = m_{e.c.}/(a/2)^3$, where $m_{e.c.}$ is the elementary cell mass and *a* is the lattice parameter.

X-ray diffraction analysis has been carried out after each annealing step. Analysis of both the full XRD patterns and individual reflections reveals that the reflex profiles broaden out as the particles size is reduced (Fig. 1).

The grain sizes, *d*, were determined using the Scherrer relation $d = \lambda/B \cos\theta$ [18]. Here $\lambda = 1.54178$ Å is the x-ray wavelength, θ is the corresponding angle of Bragg diffraction and *B* is the difference between the half-widths of a Bragg reflex of the nanopowder and a standard sample. The standard sample of Si powder with the size of 10 μm

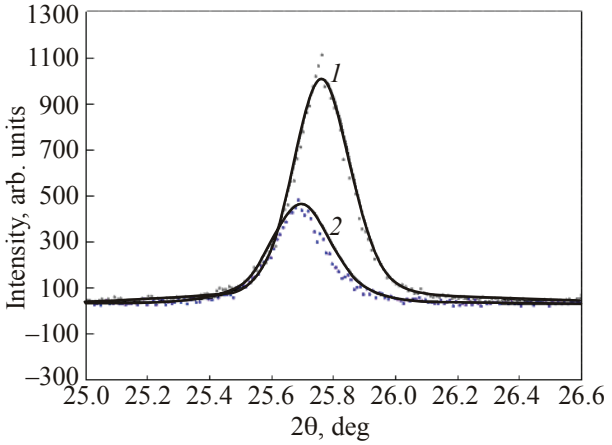

Fig. 1. Broadening of the (111) Bragg reflex of the diffraction pattern as a result of decrease of the grain size for S_3 (*1*) and S_2 (*2*) samples.

[19] was used to calibrate the intrinsic width associated to the equipment. The particle sizes were calculated using the (111) reflections of the experimental x-ray diffraction pattern and the following three relations:

1) $B_1 = \beta - \beta_0$,

where β is the half-widths of the Bragg reflex of the investigated sample and β_0 is the similar value for the Si powder,

2) $B_2 = \sqrt{\beta^2 - \beta_0^2}$,

3) $B_3 = \sqrt{(\beta - \beta_0)\sqrt{\beta^2 - \beta_0^2}}$.

The grain size values, $d(S_i)$, of $TbMnO_3$ nanopowders calculated using these relations and BET's method are listed in Table 2. Presented data indicate that the average grain sizes calculated by two methods are close to each other and increase with increasing annealing temperature.

Table 2. Particle sizes of $TbMnO_3$ nanopowders calculated using the Scherrer relation, $d(S_{XRD})$, and BET's method, $d(S_{SS})$. <*B*> is the average grain size

Sample	Particle size from XRD, $d(S_{XRD})$, nm				Particle size from BET, $d(S_{SS})$, nm
	B_1	B_2	B_3	<*B*>	<*d*>
S_2	83	64	66	70	58
S_3	49	43	44	45	40

The dc susceptibility of nanoparticle and polycrystalline samples was measured with a SQUID magnetometer at temperatures of 2–300 K in magnetic fields up to 50 kOe.

The measurements of specific heat of the $TbMnO_3$ sample composed of nanosize particles were performed by means of the relaxation method over the temperature range 2–275 K in zero magnetic field using a specific heat option of the Quantum Design PPMS.

3. Experimental results

Comparison of the temperature dependence of susceptibility, $\chi(T)$, for polycrystalline and nanoparticle samples presented in Fig. 2,*a* shows that the $\chi(T)$ dependences for all the samples are similar. The $\chi(T)$ peak corresponding to the magnetic phase transition in the Tb^{3+} sublattice decreases and broadens in the nanoparticle samples. The AFM ordering temperature for the Tb subsystem (T_N^{Tb}) was found to be depended slightly on the grain sizes (Table 3).

The analysis of high-temperature susceptibility of the samples studied was performed using the Curie–Weiss (CW) law:

$$\chi(T) = \chi_0 + \frac{C}{T - \theta}, \qquad (1)$$

where χ_0 is the background susceptibility, the Curie constant

$$C = \frac{1}{3k_B}\mu_{\text{eff}}^2, \quad \mu_{\text{eff}} = \sqrt{\left(\mu_{\text{eff}}^{\text{Tb}}\right)^2 + \left(\mu_{\text{eff}}^{\text{Mn}}\right)^2} = 10.9\,\mu_B$$

is the total effective magnetic moment,

$$\mu_{\text{eff}}^{\text{Tb}} = \mu_B g_J \sqrt{J(J+1)} = 9.7\,\mu_B$$

and

$$\mu_{\text{eff}}^{\text{Mn}} = \mu_B\, g\sqrt{S(S+1)} = 4.9\,\mu_B$$

are the Tb^{3+} and Mn^{3+} ions magnetic moments, respectively, with $g_J = 3/2$, $g = 2$ and $S = 2$, $J = 6$, θ is the paramagnetic CW temperature. The fitting of the experimental $1/\chi(T)$ dependences to the CW law (Fig. 2,*b*) shows that in a interval of temperatures from 50 to 300 K the temperature dependences of the reciprocal magnetic susceptibility are linear and obey the CW law with the negative θ values indicating that antiferromagnetic interactions are dominant. A deviation of the $1/\chi(T)$ dependences from the CW law below 50 K is connected with the magnetic ordering of the Mn^{3+} moments close to this temperature. However, the

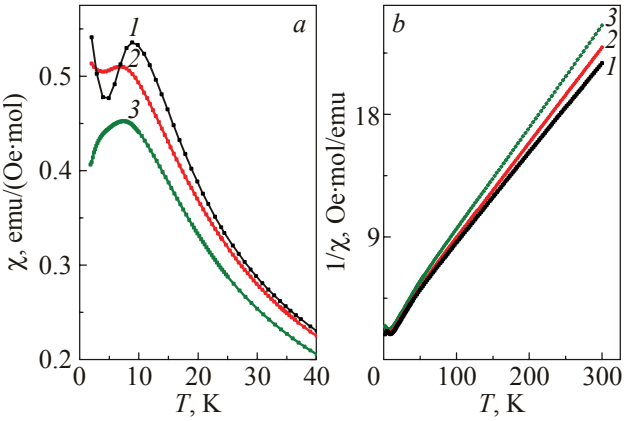

Fig. 2. (Color online) Comparison of temperature dependences of susceptibility (*a*) and reverse magnetic susceptibility (*b*) for the S_1 (*1*), S_2 (*2*) and S_3 (*3*) samples.

large Tb^{3+} magnetic moment does not allow to detect the magnetic ordering in the Mn-sublattice. The χ_0, C, θ, T_N and μ_{eff} values for the samples studied are summarized in Table 3. As seen in Table 3, the parameters calculated do not change essentially with changing the grain sizes. The μ_{eff} values of the samples studied are close to theoretical effective magnetic moment of $\mu_{eff} = 10.9\ \mu_B$ for the system with Mn^{3+} and Tb^{3+} ions. The contribution of Mn^{3+} subsystem in magnetization increases with increasing particle sizes.

Table 3. The Nèel temperatures and parameters obtained by fitting of experimental susceptibility to the Curie–Weiss law at 60–300 K

Sample	χ_0, emu/(Oe·mol)	C, emu·K/(Oe·mol)	θ, K	μ_{eff}, μ_B	T_N^{Tb}, K
S_1	0.002	14.30	–24.8	10.7	9.0
S_2	0.002	13.51	–23.0	10.4	7.4
S_3	0.0001	13.09	–26.4	10.2	7.3
Single crystal [2]					7.0

The interesting information on the magnetic properties of $TbMnO_3$ was obtained by measuring the magnetization isotherms. In Fig. 3 $M(H)$ isotherms for the S_1, S_2 and S_3 samples measured at different temperatures in magnetic field up to 50 kOe are presented.

It is seen that the magnetization does not achieve a saturation in magnetic field up to 50 kOe and decreases with decreasing sintering temperature, i.e., with reduction of $\langle d \rangle$. The magnetic moments at 2 K in magnetic field of 50 kOe are equal to 4.14, 3.65, and 3.50 μ_B/[f.u.] for the S_1, S_2 and S_3 samples, respectively. The decrease of magnetization with reducing the particle size is due to disordered surface shell of nanoparticles [13]. Supposing that the particle outermost shell has a large spin disorder and has no net moment, the decrease of the magnetic moment

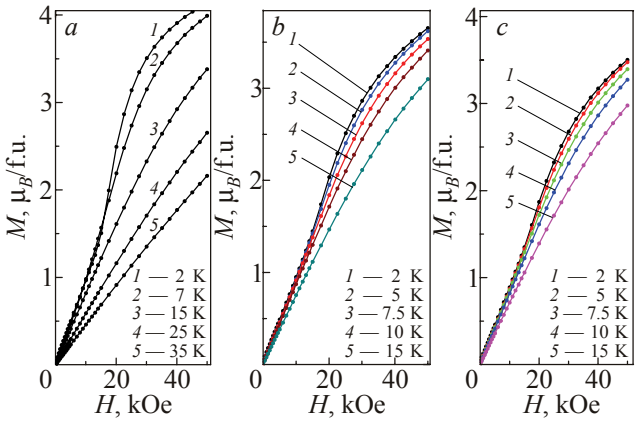

Fig. 3. (Color online) $M(H)$ isotherms for the S_1 (*a*), S_2 (*b*) and S_3 (*c*) samples measured at different temperatures.

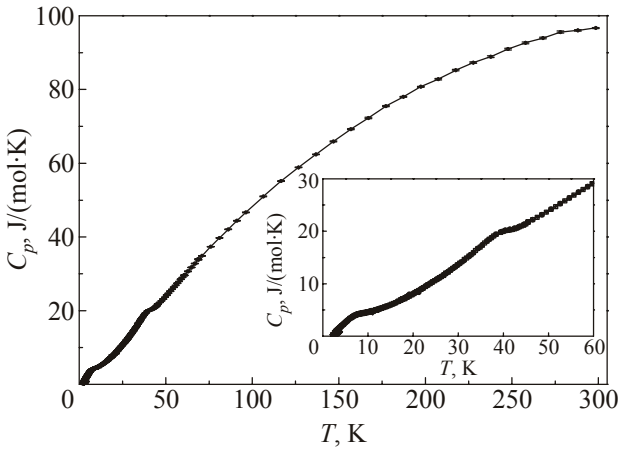

Fig. 4. Temperature dependence of the specific heat for the nanosize S_3 sample.

with reducing $\langle d \rangle$ can be explained as a result of increase of relative contribution of the surface shells to overall magnetization. In all the samples, the $M(H)$ dependences exhibit the peculiarity manifesting itself as the change of the $M(H)$ curves slope below 7.5 K in magnetic field above 17 kOe which are caused evidently with the magnetic field-induced phase transition (spin-flop type) in the rare earth sublattice. The slope of the $M(H)$ curves become distinct with decreasing temperature.

Figure 4 shows that the specific heat of the $TbMnO_3$ sample composed of nanosize particles as a function of temperature has the slightly pronounced anomalies at 7.5 and 42 K, which according to Refs. 7, 8 can be attributed to the antiferromagnetic ordering of the Tb^{3+} and Mn^{3+} moments, respectively.

For comparison with polycrystalline and nanoparticle samples, the magnetic properties of the $TbMnO_3$ film, 150 nm thick, grown onto the single crystal [001] $SrTiO_3$ substrate using magnetron sputtering technique, were studied. Temperature dependence of susceptibility, M/H, of the $TbMnO_3$ film in magnetic field of 600 Oe is presented in Fig. 5. The diamagnetic contribution arising from the substrate measured in a separate experiment was subtracted

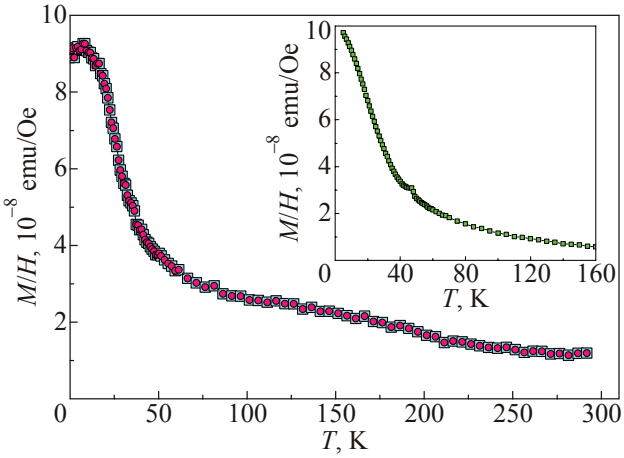

Fig. 5. Temperature dependence of M/H for the $TbMnO_3$ film. Inset: Anomaly of $M/H(T)$ near 45 K.

from the raw magnetization. The M/H dependence shows a distinct anomaly at 7.4 K and slight anomaly at 45 K (inset to Fig. 5) which are close to the anomalies of $C(T)$ dependences observed in nanoparticle specimens and correspond to the magnetic phase transitions in the Tb^{3+} and Mn^{3+} sublattices, respectively. However, the $C(T)$ and M/H dependences do not detect the anomaly at 27 K connected with an occurrence of the ferroelectric phase, followed by an incommensurate to commensurate magnetic phase transition in the Mn sublattice observed in the single crystal [2].

The hysteretic behavior in the $TbMnO_3$ film was also observed at low temperatures in the field range of ± 20 kOe. The coercive field and remanent magnetization are equal to $H_C = 2$ kOe and $M_R = 2 \cdot 10^{-4}$ emu, respectively, at $T = 5$ K. These measurements confirm that an antiferromagnetic $TbMnO_3$ exhibits an intrinsic ferromagnetic order at low temperatures [10]. One of possible origin of the observed ferromagnetism in thin film is presumed to be the coupling between magnetization and strain imposed by the substrate [11].

4. Conclusions

In this paper, the x-ray diffraction, susceptibility, magnetization and specific heat measurements of $TbMnO_3$ have been carried out. The samples were prepared by the various methods, namely, as polycrystal and two nanoparticle specimens synthesized with a sol-gel method at temperatures of 800 and 900 °C. The nanoparticle size effect on properties of $TbMnO_3$ was studied. The orthorhombic crystal structure parameters change insignificantly with decreasing grain sizes. The magnetization of the Tb^{3+} sublattice in nanospecimens is different from magnetization of the polycrystalline sample decreasing with reducing particle size. Taking into account that the nanoparticles are composed of an inner core with physical properties similar to the bulk and an outer shell with oxygen vacancies, defects and etc., a simplest explanation of the magnetic moment reduction is the existence of a noncollinear spin structure in the surface shells of nanoparticles as a result of the atom disorder.

The samples studied were found to exhibit several anomalies related to the magnetic phase transitions. Taking into account the results presented in Refs. 7, 8, the anomalies at 7.5–9 K are attributed to the magnetic ordering of the Tb^{3+} subsystem and the anomalies at $T_N^{Mn} = 42$–45 K take place as a result of ordering of the Mn^{3+} moments. The behavior of the $M(H)$ dependence below 7.5 K in magnetic field above 17 kOe is characteristic of the magnetic field-induced metamagnetic phase transition (spin-flop type).

1. M. Fiebig, *J. Phys.* ***D*****38**, R 123 (2005).
2. T. Kimura, T. Goto, H. Shitani, K. Ishizaka, T. Arima, and Y. Tokura, *Nature* **426**, 55 (2003).
3. T. Goto, T. Kimura, G. Lawes, A.P. Ramirez, and Y. Tokura, *Phys. Rev. Lett.* **92**, 257201-4 (2004).
4. T. Kimura, G. Lawes, T. Goto, Y. Tokura, and A.P. Ramirez, *Phys. Rev.* **B71**, 224425 (2005).
5. T. Goto, Y. Yamasaki, H. Watanabe, T. Kimura, and Y. Tokura, *Phys. Rev.* **B72**, 220403-R (2005).
6. F. Scherettle, P. Lunkenheimer, J. Hemberger, V.Yu. Ivanov, A.A. Mukhin, A.M. Balbashov, and A. Loidl, *Phys. Rev. Lett.* **102**, 207208 (2009).
7. M. Kenzelmann, A.B. Harris, S. Jonas, C. Broholm, J. Schefer, S.B. Kim, C.L. Hang, S.-W. Cheong, O.P. Vajk, and J.W. Lynn, *Phys. Rev. Lett.* **95**, 087206 (2005).
8. D.N. Argyriou, N. Aliouane, J. Strempfer, I. Zegkinoglou, B. Bohnenbuck, K. Habicht, and M.v. Zimmermann, *Phys. Rev.* **B75**, 02010-R (2007).
9. M. Mostovoy, *Phys. Rev. Lett.* **96**, 067601 (2006).
10. B.J. Kirby, D. Kan, A. Luykx, M. Murakami, D. Kundaliya, and I. Takeuchi, *J. Appl. Phys.* **105**, 07D917 (2009).
11. D. Rubi, C. de Graaf, C.J.M. Daumont, D. Mannix, R. Broer, and B. Noheda, *Phys. Rev.* **B79**, 014416 (2008).
12. L.I. Balcells, J. Fontcuberta, B. Martinez, and X. Obradors, *Phys. Rev.* **B58**, R14697 (1998).
13. M.A. Lopez-Quintela, L.E. Hueso, J. Rivas, and F. Rivadulla, *Nanotechnology* **14**, 212 (2003).
14. S. Roy, I. Dubenko, D.D. Edorh, and N. Ali, *J. Appl. Phys.* **96**, 1202 (2004).
15. Y.W. Duan, X.L. Kou, and J.G. Li, *Physica B: Condens. Matter* **355**, 250 (2005).
16. J. Rodriguez-Carvajal, *Physica B: Condens. Matter* **192**, 55 (1993).
17. S. Brunauer, P.H. Emmett, and E. Teller, *J. Am. Chem. Soc.* **60**, 309 (1938).
18. B.D. Cullity, *Elements of x-ray Diffraction*, Addison–Wesley, Reading, MA (1978).
19. S.D. Rasberry, *Bureau of Standards Certificate — Standard Reference Material* 640b (1987).